Enhanced Performance of Intensity Modulation With Direct Detection Using Golay Encoded Nyquist Pulses and Electronic Dispersion Compensation

Julien Moussa H. Barakat, *Senior Member, IEEE*, Abdul Rahman El Falou, Zeynep Nilhan Gürkan, Shadi A. Alboon, *Senior Member, IEEE*, and Abdullah S. Karar, *Senior Member, IEEE*

***Abstract*—The performance of intensity modulation (IM) with direct detection (DD) transmission systems is enhanced through a novel combination of multidimensional coding, Nyquist pulse shaping, and electronic dispersion compensation (EDC) at the transmitter using a finite impulse response (FIR) filter. A 24-dimensional (24D) extended Golay binary code effectively transforms each incoming 12-bit message into a 24-bit codeword, achieving a coding efficiency of 0.5 bits per symbol for a 56 Gb/s on-off keying (OOK) transmission over 80 km of single mode fiber. While this encoding process introduces a 50% overhead, the required bandwidth is maintained at 56 GHz through doubling the symbol rate and the application of Nyquist pulse shaping with a raised cosine (RC) profile and a roll-off factor of zero, resulting in a flat power spectral density. This flat distribution contrasts with standard OOK transmission at 56 Gb/s with a roll-off factor of 1.0, where signal power is predominantly concentrated in the lower frequency range. One of the key advantages of the 24D Golay code is its substantial error correction capability. However, the benefits of this multidimensional coding and Nyquist pulse shaping extend beyond error correction. It is shown that, while both the proposed and standard OOK methods exhibit comparable performance in a white Gaussian noise channel at back-to-back, they differ significantly under frequency selective power fading conditions caused by the interplay of chromatic dispersion (CD) and direct detection. The misalignment between the frequency notches introduced by the FIR pre-EDC and those inherent in the channel response, especially severe at lower frequencies, favors transmission schemes with a flat power spectral density, like the 24D Golay-coded Nyquist pulses.**

***Index Terms*—Multidimensional coding, nyquist pulse shaping, electronic dispersion compensation, intensity modulation, direct detection transmission, finite impulse response filter.**

I. Introduction

THE surge in cloud services and edge computing has markedly amplified data flows into and out of data centers, as well as within access networks. This escalation necessitates scalable and economical network infrastructures to manage, transmit, and store substantial data volumes across data centers, metro-links, and access networks. This need arises from the exponential increase in global network traffic. Optical interconnects have gained significant research interest as a vital component for ensuring end-to-end energy-efficient solutions in network infrastructures. They are favored for their high throughput, low latency, and reduced energy consumption compared to current networks reliant on active optical cables [1]. Particularly, for short-reach applications spanning 10 km to 100 km, optical interconnects predominantly employ intensity modulation (IM) at the transmitter (Tx) and direct detection (DD) at the receiver (Rx). This choice is driven by the stringent demands for low cost and energy efficiency in these applications [2].

Fiber loss and chromatic dispersion (CD) are primary factors impairing fiber communications. CD, the dominant issue in short-reach optical communications, occurs when different frequencies within a signal propagate at varying speeds. This phenomenon, similar to modal dispersion, can severely limit transmission reach due to inter-symbol interference (ISI), where one symbol begins to overlap with adjacent ones in time. Various methods, including optical domain dispersion management, electric/digital dispersion compensation, and joint optoelectronic approaches, have been developed to mitigate ISI caused by CD [3].

While coherent detection enables the recovery of the complex optical field and thus allows for straightforward compensation of chromatic dispersion (CD), intensity modulation and direct detection (IM/DD) are gaining recognition as more practical alternatives for high-speed, cost-efficient systems due to their simpler detection mechanisms. However, IM/DD systems face significant performance degradation due to linear and nonlinear forms of ISI, exacerbated by CD interaction with square-law photo-detection [4]. CD, although a linear effect, causes severe ISI in combination with DD, as linear effects turn nonlinear after square-law detection. The interaction of CD with square-law detection in IM/DD systems, typically under double side-band signal transmission, leads to power fading and substantial ISI, affecting adjacent symbols [5]. The Tx-to-Rx transfer function shows frequency-selective power fading dips as the linear component of the ISI, with nonlinear ISI arising from signal-to-signal

Manuscript received 16 January 2024; revised 19 March 2024; accepted 5 April 2024. Date of publication 9 April 2024; date of current version 19 April 2024. *(Corresponding authors: Abdullah S. Karar.)*

Julien Moussa H. Barakat, Zeynep Nilhan Gürkan, and Abdullah S. Karar are with the College of Engineering and Technology, American University of the Middle East, Kuwait (e-mail: abdullah.karar@aum.edu.kw).

Abdul Rahman El Falou is with the Department of Electrical and Computer Engineering, Beirut Arab University (BAU), Beirut 1107 2809, Lebanon.

Shadi A. Alboon is with the Department of Electronics Engineering, Hijjawi Faculty for Engineering Technology, Yarmouk University, Irbid 21163, Jordan.

Digital Object Identifier 10.1109/JPHOT.2024.3386818

beating interference (SSBI) and photodiode current power expansion [6].

Dispersion compensation in optical systems, achieved through the use of dispersion compensation modules (DCM), dispersion compensation fiber (DCF), conventional Bragg gratings, and chirped fiber Bragg gratings, effectively mitigates dispersion issues. However, this approach necessitates the integration of cumbersome components, which complicates the existing optical link by adding bulkiness and increasing cost and complexity. Alternatively, electronic dispersion compensation (EDC) methods, such as time-domain equalization (TDE), frequency-domain equalization (FDE), and least mean square (LMS) adaptive equalization, offer a cost-effective solution for compensating chromatic dispersion (CD) without the need to alter the physical fiber link [7]. EDC employs digital filters in both time and frequency domains, with digital signal processing (DSP) offering minimal modifications to existing systems [7].

Recently, an optical imaging-derived Gerchberg-Saxton (GS) iterative DSP approach has demonstrated potential in linearizing the IM/DD channel, as explored in [8], [9], [10]. The GS method uses multiple real-valued intensity image planes to iteratively extract a complex-valued optical field, enabling linear reception of optical signals in IM/DD systems. Additional dispersive devices are employed to create the necessary image planes for implementing the GS algorithm in these systems [11]. This approach linearizes the IM/DD channel effect by optimizing the optical amplitude at the transmitter to counteract CD-induced power fading and nonlinear distortion. To enhance efficiency, modifications like zero-padding and phase induction have been proposed for the GS algorithm, aimed at reducing complexity and accelerating convergence [12], [13], [14]. The GS algorithm has also been implemented as a data-aided decision-directed equalizer at the receiver [15], and a multi-constraint version was experimentally reported [11]. Recently, an implementation of the Gerchberg-Saxton (GS) algorithm using a finite impulse response (FIR) filter at the transmitter has shown promising results in mitigating power-fading ISI. The theoretical specifications of the GS-FIR filter are detailed in [16], with its first experimental demonstration reported in [17], [18].

In this work, IM/DD transmission system performance and reach is enhanced by integrating advanced signal processing techniques, including multidimensional coding, Nyquist pulse shaping, and electronic dispersion compensation using a GS-based FIR filter. At its core is the use of a 24-dimensional (24D) extended Golay binary code, which increases coding efficiency while maintaining bandwidth requirements using Nyquist pulse shaping. This method, notably different from traditional approaches, offers improved error correction and resilience, particularly under conditions of frequency selective power fading caused by chromatic dispersion and direct detection, when coupled with FIR pre-EDC.

This paper is structured in the following manner: Section II elucidates the principles of operation underlying the multi-dimensional coding coupled with Nyquist pulse shaping. In Section III, we detail the architecture of the IM/DD link, including the transmitter (Tx) and receiver (Rx) digital signal processing (DSP). The simulation results, along with a comparative analysis and discussion, are presented in Section IV. The paper concludes with Section V, summarizing the key findings and implications.

II. Principle of Operation

In coherent communication systems it is possible to use the in-phase (I) and quadrature (Q) components of the electric field in both X and Y polarizations to send multi-dimensional modulation formats for a spectral efficiency (SE) greater than 1 b/symbol. Fundamentally, the dual-polarization complex-field control at the transmitter enables the independent manipulation of $[I_x, Q_x, I_y, Q_y]$, which is a total of 4-dimensions. In order to further increase the number of orthogonal dimensions, two or more adjacent time slots or non-overlapping frequency domain subcarriers could be used provided low inter-symbol interference. Also, muiltilevel modulation using orthonormal basis functions such as n-level pulse amplitude modulation and higher order QAM can also be utilized to increase the number of bits per symbol and hence the spectral efficiency. These schemes leverage multi-dimensional signal spaces for increased bit rates. However, in IM/DD systems, the lack of phase information limits transmission to one dimension. This inherent constraint of IM/DD systems necessitates innovative approaches to enhance spectral efficiency and error tolerance without introducing undue complexity.

In long-haul subsea links with over 10,000 km transmission distance binary phase shift keying (BPSK) is utilized, due to its simplicity and tolerance to significant amounts of impairments and accumulated amplified spontaneous emission (ASE) noise. Although in these sub-seas transmission scenarios, the X and Y polarization and I/Q are used, fundamentally, the modulation of choice is BPSK. In a similar way, the transmission of telemetry data from the furthest object launched by humans (Voyager probes), over extremely large distances in the vacuum of space, use BPSK modulation coupled with Manchester line coding to improve clock extraction and synchronization. In both subsea and interplanetary transmission, forward error correction (FEC) is critical to reduce the bit-error-ratio (BER) to acceptable levels, in the presence of noise [19]. The advantages of using BPSK in both IM/DD and coherent systems become apparent when examining the channel capacity in bits/symbol plotted against the signal-to-noise ratio (SNR) in dB for various modulation formats, including BPSK, QPSK, 8-QAM, 16-QAM, 32-QAM, and 64-QAM as shown in Fig. 1(a), alongside the Shannon capacity limit for a Gaussian channel. A closer inspection in Fig. 1(b), particularly for the 1 b/symbol capacity of BPSK, reveals a potential SNR gain of approximately 6.5 dB. This gain could be theoretically achieved with infinite encoding and decoding efforts. Notably, this available SNR gain relative to the Shannon limit diminishes as the target capacity in bits/symbol increases. In this context, the introduction of 24D Golay coded modulation emerges as a particularly strategic choice. This advanced coding technique is uniquely positioned to capitalize on the aforementioned 6.5 dB SNR gain. Furthermore, its inherent error-correcting capabilities allow it to approach closer to the Shannon capacity limit, making it an optimal choice for systems operating at low SNR.

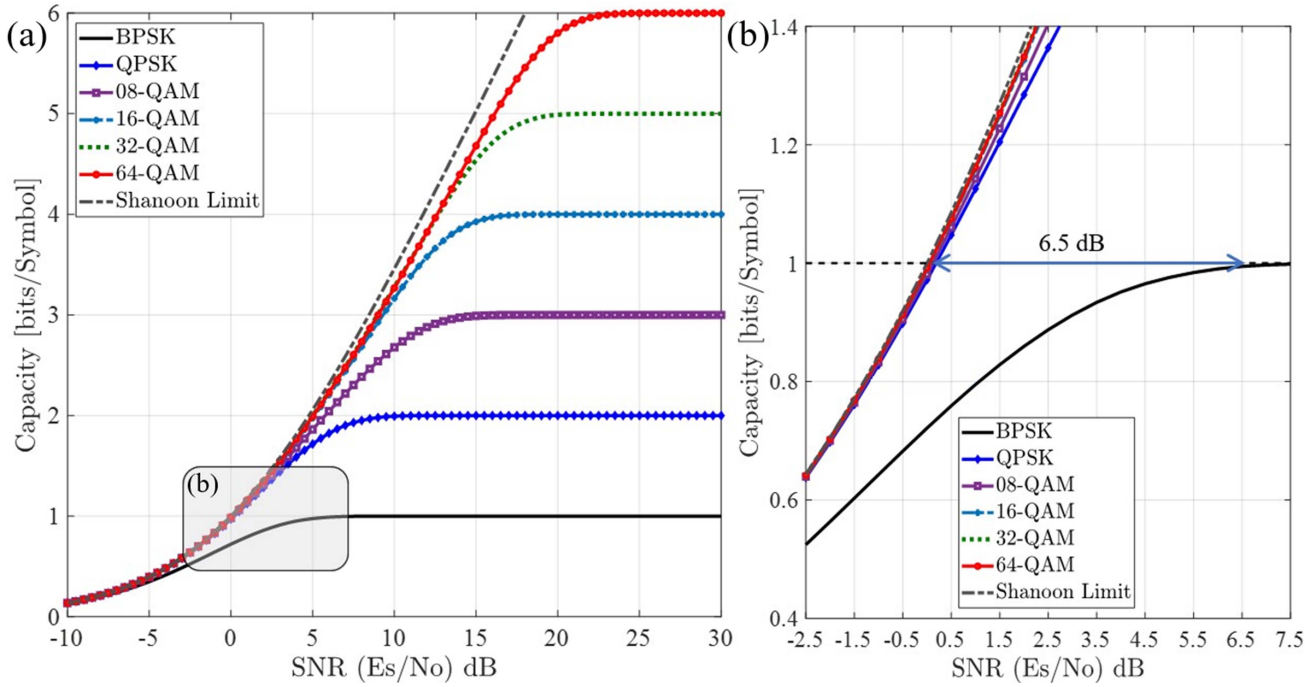

Fig. 1. Channel capacity in [bits/symbol] plotted against SNR in dB: (a) for BPSK, QPSK, 8-QAM, 16-QAM, 32-QAM, and 64-QAM, alongside the Shannon capacity limit for a Gaussian channel, (b) a focused view on the 1 b/symbol capacity for BPSK, highlighting a theoretical 6.5 dB achievable SNR gain.

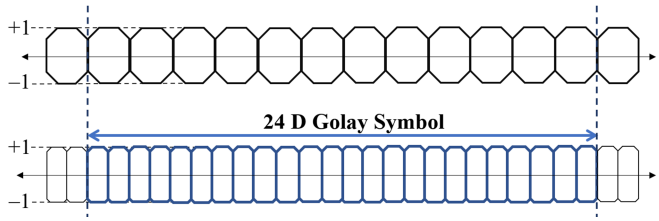

Fig. 2. Time-domain representation of a single 24D Golay symbol, encoding 12 bits at double the symbol rate relative to 12 bits of OOK modulation.

In the context of IM/DD systems, the adoption of multi-dimensional coded modulation becomes relevant. Recent advancements, such as the optimized eight-dimensional lattice modulation format for IM-DD 56 Gbit/s optical interconnections using 850 nm VCSELs, demonstrate the potential of multi-dimensional approaches in IM/DD systems [20]. The ability of 24D Golay code to correct multiple bit errors makes it a promising candidate for enhancing IM/DD system performance. Furthermore, the successful application of similar high-dimensional modulation formats in VCSEL-based IM/DD links underlines the practicality and advantages of such approaches [21].This shift from traditional BPSK to advanced 24D Golay encoded modulation supports industry efforts to enhance data throughput and reliability efficiently in data centers and short-reach interconnects.

In this study, Golay encoded modulation is introduced for IM/DD systems [21]. The need for additional bandwidth, arising from the 50% overhead characteristic of a rate 1/2 code (as detailed in the subsequent subsection), can be accommodated in two ways: by doubling the symbol rate using on-off keying (OOK) modulation, or by employing 4-ary pulse amplitude modulation (PAM-4) at the same symbol rate. This work adopts the former approach, effectively managing the increased signal bandwidth through the application of Nyquist pulse shaping and raised cosine (RC) pulse shaping with a roll-off factor of zero. Such shaping results in a wide, uniform power spectral density, which in turn, optimally utilizes the GS-based FIR pre-EDC method [17].

A. Golay Encoded Modulation

Golay codes, initially introduced in [22], have acquired significant attention in the fields of digital communications and theoretical mathematics due to theirs unique properties [23]. Both forms, binary and ternary, particularly the first variant, are central to error correction in data transmission. Their relevance extends beyond practical applications, contributing to the study of sporadic finite groups in abstract mathematics. The construction of the binary codes requires the use of binary Galois field (GF2) which supports the binary arithmetic operations. There exist two variants of the binary Golay code: The (23D) and the (24D). The first one is called the binary Golay code, denoted as [23, 12, 7] which signifies that the length of codeword is 23 bits, the message is 12 bits and the minimum distance between two binary Golay codes is 7. The codewords of [23, 12, 7] are generated using a generator polynomial. The second one is the extended binary Golay code (24D), denoted as [24, 12, 8], which is especially noteworthy in group theory. It is a linear block code with length 24, message length of 12, rate of 12/24 = 0.5, distance of 8 and a binary alphabet (size of 2). Here, we adopt the (24D) extended binary Golay Code, where the

encoding structure is robust and capable of correcting errors up to 3 bits or detecting errors up to 7 bits. It can be generated by appending a parity bit with the binary Golay code (23D) or using the associated generator matrix $G = [I_{12}\ P]$, with I_{12} being the 12 by 12 identity matrix and P given by:

$$P = \begin{bmatrix} 1 & 0 & 1 & 0 & 0 & 0 & 1 & 1 & 1 & 0 & 1 & 1 \\ 1 & 1 & 0 & 1 & 0 & 0 & 0 & 1 & 1 & 1 & 0 & 1 \\ 0 & 1 & 1 & 0 & 1 & 0 & 0 & 0 & 1 & 1 & 1 & 1 \\ 1 & 0 & 1 & 1 & 0 & 1 & 0 & 0 & 0 & 1 & 1 & 1 \\ 1 & 1 & 0 & 1 & 1 & 0 & 1 & 0 & 0 & 0 & 1 & 1 \\ 1 & 1 & 1 & 0 & 1 & 1 & 0 & 1 & 0 & 0 & 0 & 1 \\ 0 & 1 & 1 & 1 & 0 & 1 & 1 & 0 & 1 & 0 & 0 & 1 \\ 0 & 0 & 1 & 1 & 1 & 0 & 1 & 1 & 0 & 1 & 0 & 1 \\ 0 & 0 & 0 & 1 & 1 & 1 & 0 & 1 & 1 & 0 & 1 & 1 \\ 1 & 0 & 0 & 0 & 1 & 1 & 1 & 0 & 1 & 1 & 0 & 1 \\ 0 & 1 & 0 & 0 & 0 & 1 & 1 & 1 & 0 & 1 & 1 & 1 \\ 1 & 1 & 1 & 1 & 1 & 1 & 1 & 1 & 1 & 1 & 1 & 0 \end{bmatrix} \quad (1)$$

It is crucial to note that uncoded binary modulation, and the 24-Golay encoded modulation operate at differing bits-per-symbol rates. In order to fully harness the potential of 24D Golay encoded modulation, the symbol rate needs to be increased twofold compared to the binary modulation. This enhancement allows for 24 distinct time slots within a single Golay encoded symbol, a concept as illustrated in Fig. 2.

The efficacy of an error-correcting approach is often quantified by the BER for a signal that is modulated in an antipodal manner under the influence of additive white Gaussian noise (AWGN). In different scenarios, performance metrics might focus on signal energy or on bit energy, both compared against noise variance. These two metrics are interconnected, as shown by the equation:

$$\frac{E_b}{N_0} = \frac{E_s}{rN_0} \quad (2)$$

In this context, E_s signifies the energy of the signal, E_b represents the energy per bit, N_0 refers to the noise energy, and r specifies the rate of the combined modulation and coding scheme, measured in bits per second per Hertz. The graph in Fig. 3 illustrates the Monte-Carlo simulated BER plotted against the E_b/N_0 ratio. This ratio, which is analogous to E_s/N_0 adjusted for the coding rate, compares the performance of uncoded binary modulation with 24D Golay encoded modulation. The analysis includes a maximum likelihood (ML) receiver operating under both hard-decision and soft-decision decoding methods. The simulation encompasses a total of 75,000 bits to provide a comprehensive view of the decoding effectiveness. Superimposed are three error correction threshold limits: a 20% (SD-FEC) limit where BER is equal to 2×10^{-2}, a 7% (HD-FEC) limit where BER is equal to 3.8×10^{-3} and the (K4 FEC) limit where BER is equal to 2.4×10^{-4}. The utilization of 24D Golay encoded modulation offers a 2.6 dB and 3.5 dB improvement over uncoded modulation with ML soft-decision decoding at the 7% HD-FEC limit and K4-FEC limit, respectively. It is important to emphasize that the performance curves depicted in Fig. 3 solely reflect the enhancements attributed to coded modulation. They do not consider the impact of the symbol rate, which doubles in comparison to uncoded modulation.

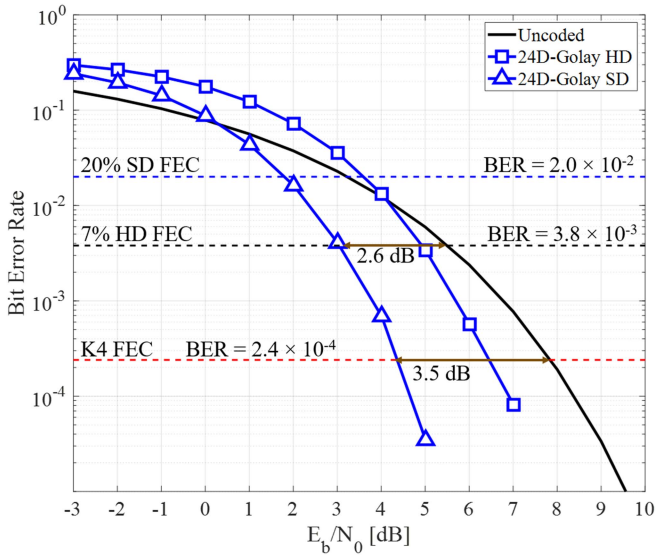

Fig. 3. Monte-Carlo simulated BER plotted against the E_b/N_0 in dB for uncoded binary modulation, and 24D Golay encoded modulation with SD and HD decoding. Superimposed are three error correction threshold limits: a 20% (SD-FEC) limit where BER $= 2 \times 10^{-2}$, a 7% (HD-FEC) limit where BER $= 3.8 \times 10^{-3}$ and the K4 FEC limit where BER $= 2.2 \times 10^{-4}$.

Remarkably, despite the higher computational complexity, SD decoding for the expanded Golay code has attracted a lot of attention since it performs noticeably better than HD decoding. In real applications, ML soft decoding typically presents computational challenges while achieving the best decoding performance. For instance, matching the received word with each of the 4,096 possible codewords is necessary for Brute-force ML decoding of the expanded Golay code. As described in references [24], [25], [26], a variety of decoding algorithms for Golay codes have been presented, catering to various contexts. Interestingly, [27] proposes a decoder design for the extended (24, 12, 8) Golay code that provides almost ideal performance (within 0.2 dB). This architecture has a throughput of one output every 24 clock cycles, a 48 clock cycle latency, and a comparatively low complexity—4,000 2-input NAND gates. Another noteworthy design is given in [28], which is based on imperfect ML (IML) decoding for the expanded Golay code. It is ideally suited for high data rate systems due to its decreased complexity of 3,000 gates, 27 clock cycle latency, and high throughput of one output per clock cycle. Furthermore, a parallel version of IML is suggested in [29], showing an remarkably low latency of 5 clock cycles and a 10% boost in throughput with the same performance as the IMLD decoder. Additionally, a real-time implementation of Tx/Rx DSP based on extended Golay coded modulation for a coherent transceiver is reported in [30].

B. *Pre-EDC Using a GS-Based FIR Filter*

In this work, the Gerchberg-Saxton algorithm, is realized through a FIR, implemented through a streamlined tap delay line structure. This structure incorporates optimal taps, which are

derived through the analytical or equivalent numerical process described in [16], [17]. The FIR approach effectively separates the pattern-dependent characteristics of transmission from the GS iterative process, focusing on a singular impulse at the DD receiver. Throughout the GS algorithm iterations, an impulse response for the GS FIR filter is generated. This response plays a crucial role in counteracting the power fading induced by ISI, as detailed in [16].

The starting point for this analysis is the normalized power fading transfer function $H(f)$ for the linear ISI IM/DD channel given by:

$$H(f) = \cos\left(2\pi^2 \beta_2 L f^2\right) \tag{3}$$

Here, $L = 80$ km denotes fiber length, the group velocity dispersion parameter β_2 is calculated using the expression: $\beta_2 = -D\lambda^2/(2\pi c)$, where c represents the speed of light, $D = 16.75$ ps/nm/km is the dispersion coefficient, and $\lambda = 1550$ nm is the wavelength of the light.

The pre-EDC FIR filter implements a transfer function obtained after m iterations of the GS algorithm $H_{GS}^{m}(f)$ is:

$$H_{GS}^{m}(f) = \frac{1 - \sin^{2m}\left(2\pi^2 \beta_2 L f^2\right)}{\cos\left(2\pi^2 \beta_2 L f^2\right)} + \sin^{2m}\left(2\pi^2 \beta_2 L f^2\right) \tag{4}$$

An examination of the experimental results in [17], reveal that the pulse shape has influence on the effectiveness of the FIR based pre-EDC. The primary distinctions among the three analyzed pulse shapes explored in [17]: - non-return-to-zero rectangular (Rect), non-return-to-zero raised cosine (RC), and return-to-zero (RZ) - are highlighted in terms of their frequency envelopes and peak-to-average power ratios (PAPRs). Although all pulse shapes utilize the full bandwidth of the transmitter (56 GHz), the distribution of the modulated signal's informational content within this bandwidth varies. Notably, the RZ pulse shape demonstrates a more uniform frequency spectrum distribution compared to Rect and RC. This uniformity results in a broader dispersion of the CD-induced null effects across the frequency range, whereas the latter two pulse shapes concentrate more signal power at lower frequencies.

It is observed in [17], that the filter's effectiveness varies across the frequency band. Ideally, the frequency null points of the GS filter, denoted as $H_{GS}^{m}(f)$ in equation (4), should align with those in the fiber transfer function in equation (3). However, this alignment is not always precise, leading to a misalignment that diminishes with an increasing frequency, and is more pronounced at lower frequencies. This phenomenon is analytically demonstrated by evaluating and comparing the roots of the transfer functions $H(f)$ and $H_{GS}^{m}(f)$. The results in Figs. 4 and 5 illustrate these effects, showing the zero-crossing points and relative error between the roots of the two functions, respectively, with $m = 15$ iterations for a specified frequency band.

III. Transmission System Set-Up

In this work, two different transmission scenarios are examined. The first is transmission of data at 56 Gbit/s OOK over 80 km of single mode fiber (SMF) using RZ, Rect, and RC pulse shaping with a roll-off factor of one, occupying a null-to-null bandwidth of 56 GHz. The second proposed scheme is 56 Gbit/s 24D Golay encoded transmission using 112 GSymble/s NRZ-OOK over 80 km of SMF using RC pulse shaping with a roll-off factor of zero (Nyquist) pulse shaping. The latter approach will be referred to as 24D Golay encoded Nyquist pulse shaping in the remainder of this paper. The simulation architecture for the IM/DD physical layer link, depicted in Fig. 6, was executed within an Optisystem/MATLAB co-simulation framework. This setup incorporated an amplitude-only EDC mechanism at the transmitter using an FIR filter, as detailed in [8], [10], [12].

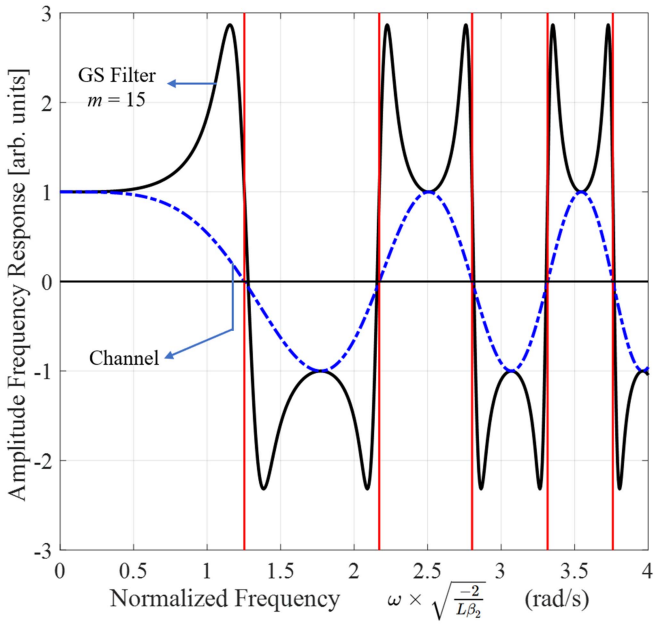

Fig. 4. Amplitude response of $H(f)$ and $H_m^{GS}(f)$ for m =15 with the zero-crossings of each function illustrated for the first 6 null points.

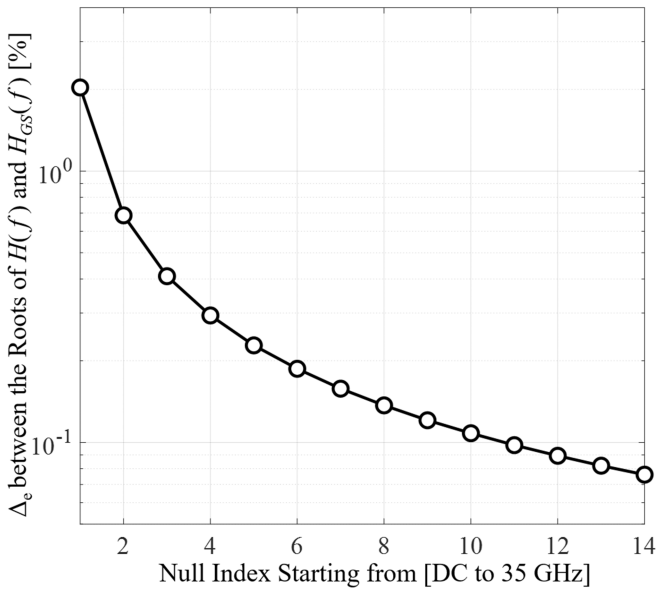

Fig. 5. Relative error between the roots of $H(f)$ and $H_m^{GS}(f)$ as a function of the counted null index starting from DC for the first 14 nulls.

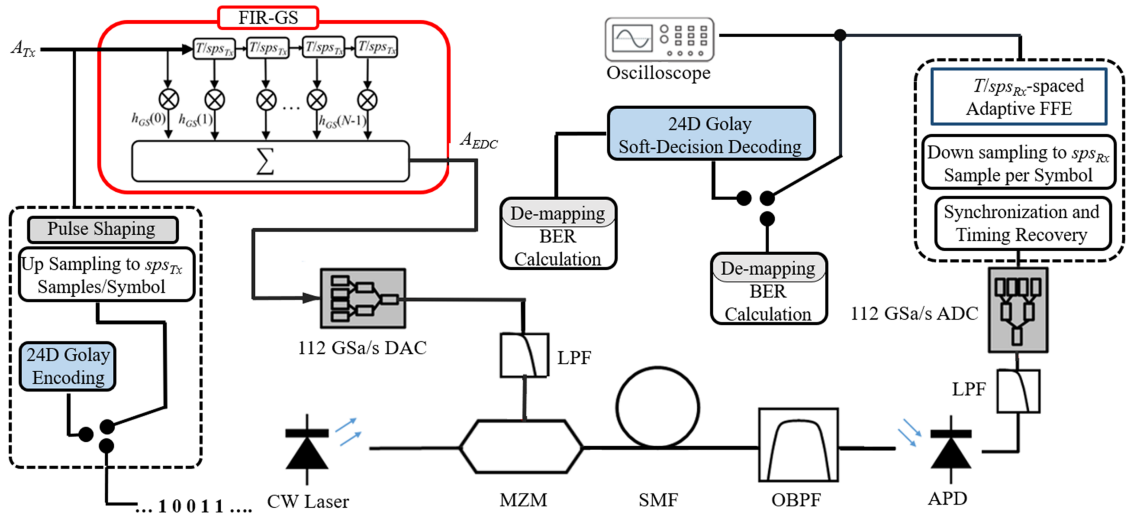

Fig. 6. System level simulation set-up with details of the DSP FIR based GS EDC algorithm at the transmitter for 56 Gbit/s OOK, and 24D Golay encoded transmission using 112 GSymb/s NRZ-OOK over 80 km of SMF.

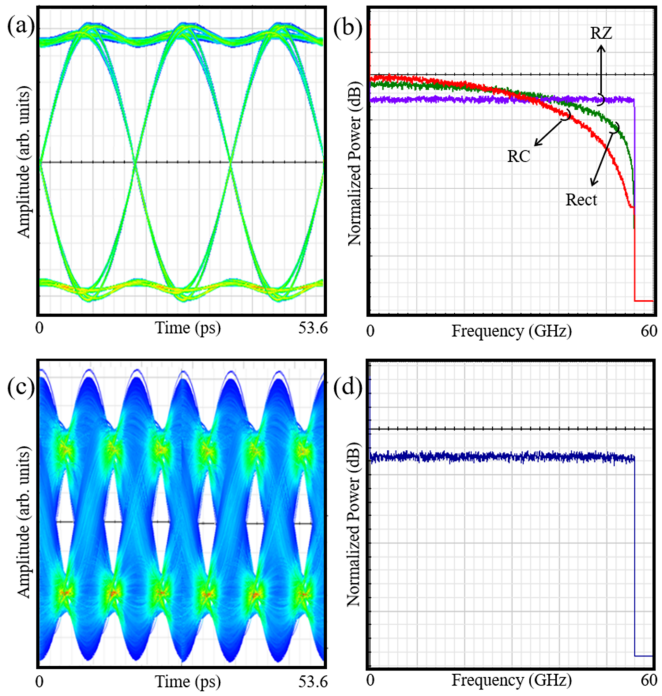

Fig. 7. Back-to-back electrical eye-diagram and RF spectrum (6 dB/div) of the transmitted signal:(a) and (b) for the 56 Gbit/s OOK [RC, Rect, RZ], (c) and (d) for the 56 Gbit/s 24D Golay encoded Nyquist pulse shaping.

The transmitter digital-to-analog converter (DAC) and receive analog-to-digital converter (ADC) are both assumed to operate at 112 GSamples/s (GSa/s) with an 8-bit resolution, resulting in a maximum controllable DC-to-null bandwidth of 56 GHz. The 56 Gbit/s OOK uses two samples-per-symbol ($sps_{Tx} = 2$ and $sps_{Rx} = 2$) at both the transmitter and receiver, while the 56 Gbit/s 24D Golay encoded transmission utilizes a single sample-per-symbol ($sps_{Tx} = 1$ and $sps_{Rx} = 1$) at both the transmitting and receiving ends. In both scenarios, the spectral constraints limit the signal to a maximum bandwidth of 56 GHz. Notably, digital RC pulse shaping with a roll-off factor of one, is only feasible for the 56 Gbit/s NRZ-OOK signal when $sps_{Tx} = 2$. To simulate transmitter bandwidth limitations, a 3rd order low-pass Gaussian electrical filter with a 60 GHz 3-dB cutoff frequency is utilized. At the transmitter, a 1025-tap FIR GS filter was utilized, and at the receiver, a 5-tap adaptive post-feed forward equalizer (FFE) was employed for compensating residual ISI.

The produced electrical signal powers a chirp-free Mach-Zehnder modulator (MZM) that produces at 2 dBm when coupled with a 1550 nm continuous wave (CW) laser. The optical link, unaided by amplifiers, includes a SMF segment with a loss of 0.2 dB/km and active fiber nonlinearity. A variable optical attenuator (VOA) that adjusts the received optical power (ROP) and a 400 GHz second-order Gaussian optical bandpass filter (OBPF) are integrated into the optical system at the receiving end. An avalanche photodiode (APD) transforms the optical signal into an electrical signal. The signal is then processed using a fifth-order Bessel electrical low-pass filter (LPF) operating at 60 GHz. Using an 8-bit 112 GSa/s ADC, the received signal is digitalized. This is followed by synchronization, timing recovery, and down-sampling to sps_{Rx} samples-per-symbol. For equalization at the receiver, a T/sps_{Rx}-spaced adaptive post-FFE is employed. In the case of 24D Golay coded Nyquist pulse shaping, the receiver employs soft-decision decoding. Analysis of the received electrical signal is performed using an oscilloscope, focusing on the eye-diagram. To reduce edge effects, the first 40,000 symbols of the transmission are set aside for training the adaptive equalizers, with 36 symbols on either end of the simulation window being ignored. The next 91,000 symbols are the payload for direct error counting bit error ratio (BER) analysis. A hard-decision (HD) forward error correction (FEC) threshold is set at a BER of 3.8×10^{-3}, equating to a quality factor of 8.5 dBQ [31]. Additionally, the KP4 FEC BER threshold of 2.4×10^{-4} is also considered [32].

IV. Results and Discussion

The back-to-back electrical eye-diagram and radio frequency (RF) spectrum of the transmitted signal is shown in Fig. 7(a) and

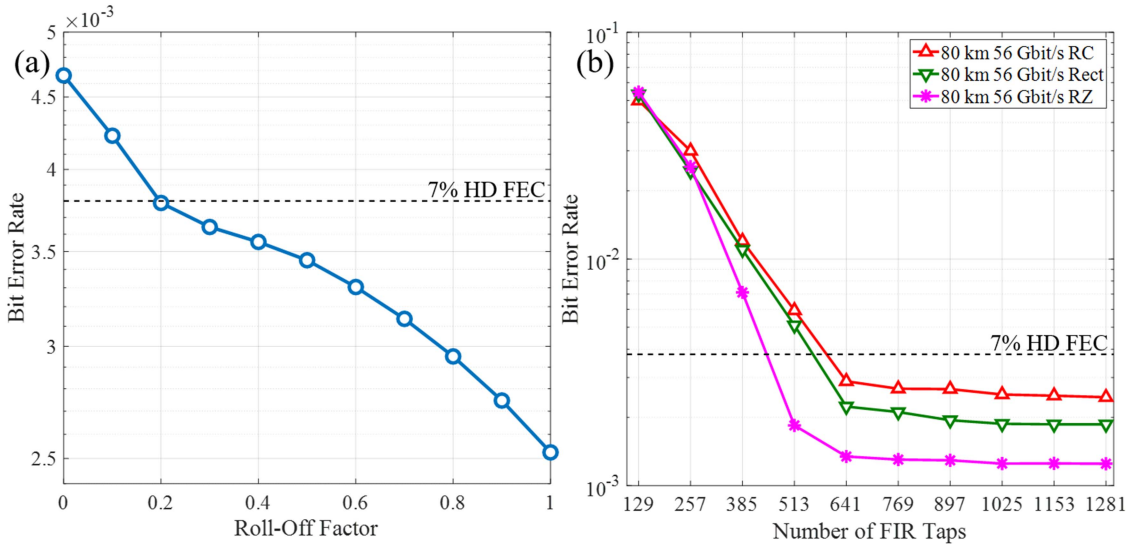

Fig. 8. Roll-off factor and number of FIR taps optimization: (a) BER versus roll-off factor for RC pulse shaping after 80 km transmission at maximum ROP, (b) BER versus number of FIR taps for RC, Rect, and RZ pulse shapes with an adaptive FFE tap count of 5.

(b) for the 56 Gbit/s OOK transmission case, and is shown in Fig. (7c) and (d) for the 56 Gbit/s 24D Golay encoded Nyquist pulse shaping transmission, respectively. The RF spectra of NRZ-OOK, depicted in Fig. 7(b), are illustrated for RC, Rect, and RZ pulse shapes. The results in Fig. 8(a) examines the impact of the roll-off factor in RC pulse shaping on BER after 80 km of transmission at maximum received optical power (ROP). An increase in the penalty due to power fading effects is observed with decreasing roll-off factors. This increase is attributed to a greater misalignment between the notch of the FIR filter and the channel responses at lower frequencies, where a higher concentration of the signal is noted, thus diminishing the benefits of FIR-based dispersion compensation for smaller roll-off factors. In Fig. 8(b), the focus is shifted to the relationship between the BER and the number of FIR pre-EDC taps, comparing RC, Rect, and RZ pulse shapes at maximum ROP, while keeping the number of adaptive FFE taps constant at five. This comparison reveals a marginal improvement with the RZ pulse shape, confirming the findings reported in [17], [33].

The BER plotted against the ROP for the 56 Gbit/s OOK [RC, Rect, RZ] and 56 Gbit/s 24D Golay encoded Nyquist pulse shaping transmission over 80 km of SMF is shown in Fig. 9. The frequency content in the 24D Golay encoded modulation exhibits a more uniform distribution. This characteristic enables the transmission system to fully leverage the advantages of the FIR-based pre-EDC. Unlike the 56 Gbit/s NRZ-OOK cases, where misalignments between the GS-based filter nulls and the channel response concentrate primarily on the signal's lower frequency content, the 24D Golay system avoids this limitation, ensuring a more balanced performance across different frequencies. The performance trends depicted in Fig. 9 suggest that increasing the symbol rate by a factor of two effectively diminishes the coding benefits of 24D Golay-encoded Nyquist pulses, particularly noticeable in the back-to-back performance at the FEC thresholds relevant to this study. When transmitted over an 80 km span of SMF, the 24D Golay-encoded Nyquist

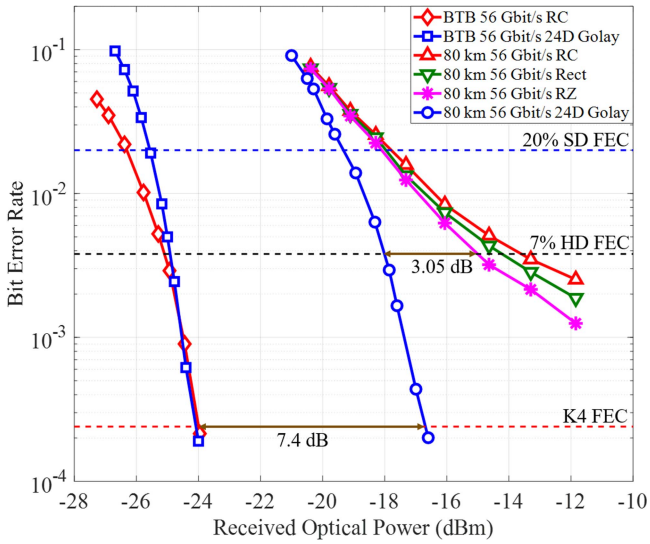

Fig. 9. BER vs ROP for the 56 Gbit/s OOK [RC, Rect, RZ] and 56 Gbit/s 24D Golay encoded Nyquist pulse shaping transmission over 80 km.

pulses demonstrate a significant margin of 3.05 dB at the 7% hard decision FEC limit, outperforming RZ-OOK. However, at the K4 FEC threshold, the system incurs a 7.4 dB penalty. In contrast, the BER performance of OOK is unable to meet this BER threshold, primarily due to the emergence of an error floor.

V. Conclusion

The integration of multidimensional coding, Nyquist pulse shaping, and EDC using a FIR filter significantly enhances the performance of IM with DD transmission systems. The implementation of a 24D extended Golay binary code, which converts 12-bit messages into 24-bit codewords, achieves a coding efficiency of 0.5 bits per symbol for 56 Gbit/s OOK transmission over 80 km of SMF. This approach, despite introducing

a 50% overhead, maintains the required 56 GHz bandwidth by doubling the symbol rate and applying Nyquist pulse shaping with a RC profile. The resultant flat power spectral density presents a stark contrast to the standard OOK transmission at 56 Gb/s, which typically exhibits a power concentration in the lower frequency range. A notable advantage of the 24D Golay code lies in its robust error correction capability. However, the study reveals that the benefits of this multidimensional coding and Nyquist pulse shaping are not confined to error correction alone. Comparative analyses under conditions of white Gaussian noise and frequency selective power fading, induced by CD and direct detection, demonstrate significant performance disparities between the proposed method and standard OOK transmission. The alignment of frequency notches introduced by FIR pre-EDC with those inherent in the channel response, particularly critical at lower frequencies, underscores the effectiveness of transmission schemes with a flat power spectral density, such as the 24D Golay-coded Nyquist pulses.

REFERENCES

[1] S. Sarmiento et al., "Split-enabled 350–630 Gb/s optical interconnect with direct detection NOMA-CAP and 7-core multi-core fiber," *Opt. Commun.*, vol. 463, no. 125321, May 2020, Art. no. 125321.

[2] M. Chagnon, "Optical communications for short reach," *J. Lightw. Technol.*, vol. 37, no. 8, pp. 1779–1797, Apr. 2019.

[3] S. M. Ranzini, R. Dischler, F. D. Ros, H. Bulow, and D. Zibar, "Experimental investigation of optoelectronic receiver with reservoir computing in short reach optical fiber communications," *J. Lightw. Technol.*, vol. 39, no. 8, pp. 2460–2467, Apr. 2021.

[4] N. Feng and X. Sun, "Hierarchical modulation PAM4 with digital nyquist pulse-shaped for flexible multi-ONU provisioning in," NG-TDM PON, *Opt. Fiber Technol.*, vol. 53, no. 102063, Dec. 2019, Art. no. 102063.

[5] L. Jiang et al., "Integrated components and solutions for high-speed short-reach data transmission," *Photonics*, vol. 8, no. 3, pp. 77–102, Mar. 2021.

[6] R. Rath, D. Clausen, S. Ohlendorf, S. Pachnicke, and W. Rosenkranz, "Tomlinson–harashima precoding for dispersion uncompensated PAM-4 transmission with direct-detection," *J. Lightw. Technol.*, vol. 35, no. 18, pp. 3909–3917, Sep., 2017.

[7] T. Xu et al., "Chromatic dispersion compensation in coherent transmission system using digital filters," *Opt. Exp.*, vol. 18, no. 15, pp. 16243–16257, Jul. 2010. [Online]. Available: http://opg.optica.org/oe/abstract.cfm?URI=oe-18-15-16243

[8] A. S. Karar, "Iterative algorithm for electronic dispersion compensation in IM/DD systems," *J. Lightw. Technol.*, vol. 38, no. 4, pp. 698–704, Feb. 2020.

[9] G. Goeger, C. Prodaniuc, Y. Ye, and Q. Zhang, "Transmission of intensity modulation-direct detection signals far beyond the dispersion limit enabled by phase-retrieval," in *Proc. Eur. Conf. Opt. Commun.*, 2015, pp. 1–3.

[10] X. Wu, A. S. Karar, K. Zhong, A. P. T. Lau, and C. Lu, "Experimental demonstration of pre-electronic dispersion compensation in IM/DD systems using an iterative algorithm," *Opt. Exp.*, vol. 29, no. 16, pp. 24735–24749, Aug. 2021. [Online]. Available: http://opg.optica.org/oe/abstract.cfm?URI=oe-29-16-24735

[11] S. Hu et al., "Multi-constraint gerchberg-saxton iteration algorithms for linearizing IM/DD transmission systems," *Opt. Exp.*, vol. 30, no. 6, pp. 10019–10031, Mar. 2022. [Online]. Available: http://opg.optica.org/oe/abstract.cfm?URI=oe-30-6-10019

[12] D. Zou, F. Li, W. Wang, M. Yin, Q. Sui, and Z. Li, "Modified Gerchberg-Saxton algorithm based electrical dispersion pre-compensation for intensity-modulation and direct-detection systems," *J. Lightw. Technol.*, vol. 40, no. 9, pp. 2840–2849, May 2022.

[13] D. Zou, W. Wang, M. Yin, Q. Sui, Z. Li, and F. Li, "Performance enhanced Gerchberg-Saxton algorithm based electrical dispersion pre-compensation for intensity-modulation and direct-detection system," in *Proc. Asia Commun. Photon. Conf.*, 2021, paper W1B.3. [Online]. Available: http://opg.optica.org/abstract.cfm?URI=ACPC-2021-W1B.3

[14] M. Yin, D. Zou, W. Wang, F. Li, and Z. Li, "Transmission of a 56-Gbit/s PAM4 signal with low-resolution DAC and pre-equalization only over 80 km fiber in C-band IM/DD systems for optical interconnects," *Opt. Lett.*, vol. 46, no. 22, pp. 5615–5618, Nov. 2021. [Online]. Available: http://opg.optica.org/ol/abstract.cfm?URI=ol-46-22-5615

[15] S. Hu, J. Zhang, J. Tang, W. Jin, R. Giddings, and K. Qiu, "Data-aided iterative algorithms for linearizing IM/DD optical transmission systems," *J. Lightw. Technol.*, vol. 39, no. 9, pp. 2864–2872, May 2021.

[16] A. S. Karar, "Gerchberg-saxton based FIR filter for electronic dispersion compensation in IM/DD transmission Part I: Theory and simulation," *J. Lightw. Technol.*, vol. 41, no. 5, pp. 1335–1345, Mar. 2023.

[17] X. Wu, A. S. Karar, K. Zhong, Z. N. Gürkan, A. P. T. Lau, and C. Lu, "Gerchberg-Saxton based FIR filter for electronic dispersion compensation in IM/DD transmission Part II: Experimental demonstration and analysis," *J. Lightw. Technol.*, vol. 41, no. 5, pp. 1428–1435, Mar. 2023.

[18] X. Wu, J. Zhang, A. P. T. Lau, and C. Lu, "C-band 100-GBaud PS-PAM-4 transmission over 50-km SSMF enabled by FIR-filter-based pre-electronic dispersion compensation," *Opt. Exp.*, vol. 31, no. 11, pp. 17759–17768, May 2023. [Online]. Available: https://opg.optica.org/oe/abstract.cfm?URI=oe-31-11-17759

[19] S. Jia, "Forward error correction (FEC): A primer on the essential element for optical transmission interoperability," *CableLabs*, Apr. 2019. [Online]. Available: https://www.cablelabs.com/insights/forward-error-correction-fec

[20] X. Lu, A. Tatarczak, V. Lyubopytov, and I. T. Monroy, "Optimized eight-dimensional lattice modulation format for IM-DD 56 Gb/s optical interconnections using 850 nm VCSELs," *J. Lightw. Technol.*, vol. 35, no. 8, pp. 1407–1414, Apr. 2017.

[21] X. Lu, V. S. Lyubopytov, and I. T. Monroy, "24-Dimensional modulation formats for 100 Gbit/s IM-DD transmission systems using 850 nm single-mode VCSEL," in *Proc. Eur. Conf. Opt. Commun.*, 2017, pp. 1–3.

[22] M. J. Golay, "Notes on digital coding," *Proc. Inst. Radio. Eng.*, vol. 37, no. 6, p. 657, 1949.

[23] F. J. MacWilliams and N. J. A. Sloane, *The Theory of Error-Correcting Codes*. Amsterdam, The Netherlands: Elsevier, 1983.

[24] J. Conway and N. Sloane, "Soft decoding techniques for codes and lattices, including the Golay code and the leech lattice," *IEEE Trans. Inf. Theory*, vol. 32, no. 1, pp. 41–50, Jan. 1986.

[25] A. Vardy and Y. Be'ery, "More efficient soft decoding of the Golay codes," *IEEE Trans. Inf. Theory*, vol. 37, no. 3, pp. 667–672, May 1991.

[26] T.-C. Lin, H.-C. Chang, H.-P. Lee, and T.-K. Truong, "On the decoding of the (24,12,8) Golay code," *Inf. Sci.*, vol. 180, no. 23, pp. 4729–4736, 2010. [Online]. Available: https://www.sciencedirect.com/science/article/pii/S0020025510003889

[27] P. Adde and R. L. Bidan, "A low-complexity soft-decision decoding architecture for the binary extended Golay code," in *Proc. IEEE 19th Int. Conf. Electronics, Circuits, Syst.*, 2012, pp. 705–708.

[28] S. Sarangi and S. Banerjee, "Efficient hardware implementation of encoder and decoder for Golay code," *IEEE Trans. Very Large Scale Integration Syst.*, vol. 23, no. 9, pp. 1965–1968, Sep. 2015.

[29] P. Zhang, F. C. M. Lau, and C.-W. Sham, "Design of a high-throughput low-latency extended Golay decoder," in *Proc. 23 rd Asia-Pacific Conf. Commun.*, 2017, pp. 1–4.

[30] T. Zeng, L. Meng, J. Li, M. Luo, X. Li, and L. Huang, "Real time coherent transceiver based on 12-bits 24 dimensions Golay coded modulation," in *Proc. Eur. Conf. Opt. Commun.*, 2018, pp. 1–3.

[31] A. Tychopoulos, O. Koufopavlou, and I. Tomkos, "FEC in optical communications - A tutorial overview on the evolution of architectures and the future prospects of outband and inband FEC for optical communications," *IEEE Circuits Devices Mag.*, vol. 22, no. 6, pp. 79–86, Nov./Dec., 2006.

[32] IEEE Standard for Ethernet - Amendment 10: Media Access Control Parameters, Physical Layers, and Management Parameters for 200 Gb/s and 400 Gb/s Operation, IEEE Standard 802.3bs-2017 (Amendment to IEEE 802. 3- 2015 as amended by IEEE's 802.3bw-2015, 802.3by-2016, 802.3bq-2016, 802.3bp-2016, 802.3br-2016, 802.3bn-2016, 802.3bz-2016, 802.3bu-2016, 802.3bv-2017, and IEEE 802.3-2015/Cor1-2017), 2017.

[33] X. Wu, J. Zhang, A. P. T. Lau, and C. Lu, "C-band 120-Gb/s PAM-4 transmissions over a 100-km dispersion-uncompensated SSMF using joint combined pulse shaping and low-complexity nonlinear equalization," *Opt. Lett.*, vol. 47, no. 19, pp. 5144–5147, Oct. 2022. [Online]. Available: https://opg.optica.org/ol/abstract.cfm?URI=ol-47-19-5144